Available online at www.sciencedirect.com
ScienceDirect
Solid State Communications 142 (2007) 190–194
solid state communications
www.elsevier.com/locate/ssc

Synthesis and magnetic properties of Mn doped ZnO nanowires

Sasanka Deka, P.A. Joy*

Physical and Materials Chemistry Division, National Chemical Laboratory, Dr. Homi Bhabha Road, Pune 411008, India

Received 15 November 2006; received in revised form 12 February 2007; accepted 14 February 2007 by J. Fontcuberta
Available online 17 February 2007

Abstract

Mn doped ZnO nanowires have been synthesized using a simple autocombustion method. The as-synthesized Mn doped ZnO nanowires were characterized by X-ray diffraction and transmission electron microscopy. An increase in the hexagonal lattice parameters of ZnO is observed on increasing the Mn concentration. Optical absorption studies show an increment in the band gap with increasing Mn content, and also give evidence for the presence of Mn^{2+} ions in tetrahedral sites. All $Zn_{1-x}Mn_xO$ ($0 \leq x \leq 0.25$) samples are paramagnetic at room temperature. However, a large increase in the magnetization is observed below 50 K. This behavior, along with the negative value of the Weiss constant obtained from the linear fit to the susceptibility data below room temperature, indicate ferrimagnetic behavior. The origin of ferrimagnetism is likely to be either the intrinsic characteristics of the Mn doped samples, or due to some spinel-type impurity phases present in the samples that could not be detected.

PACS: 75.50.Pp; 75.60.-d; 78.40.Fy

Keywords: A. Diluted magnetic semiconductor; A. Mn doped ZnO; B. Combustion synthesis; D. Magnetic properties

1. Introduction

Studies on ZnO based diluted magnetic semiconductors (DMSs) have received much attention in the recent years after Sato et al. first predicted that ZnO doped with 3d transition metal ions such as V, Cr, Fe, Co, and Ni may exhibit ferromagnetism [1]. Dietl et al. also predicted that Mn doped p-type ZnO should be ferromagnetic above room temperature [2]. Based on these predictions, several experimental investigations have been carried out by different researchers on ZnO based DMSs [3,4]. There are many studies reported on ZnO based DMSs on thin film samples fabricated using different techniques, as well as on polycrystalline materials synthesized by different methods. It is generally believed that the origin of ferromagnetism in such transition metal doped ZnO is carrier induced. No ferromagnetic ordering has been observed for Cr to Cu doped ZnO thin film samples, down to 3 K, in the earlier studies made by Jin et al. in 2001 [5]. From studies on thin film samples, Fukumura et al. showed a 36% solubility of Mn in ZnO, with strong antiferromagnetic ordering [6]. However, recently Coey et al. found room temperature ferromagnetism in some of these transition metal ion doped ZnO thin films [7]. In fact, in a very recent report, Hong et al. showed that Zn site defects in ZnO thin films give rise to room temperature ferromagnetism, and there is no role for the doped transition metals such Mn and Fe in introducing magnetism in the ZnO lattice [8].

The presence or absence of ferromagnetism, either at room temperature or at low temperatures, in polycrystalline Mn doped ZnO, has been reported by various research groups. Kolesnik et al. first synthesized polycrystalline Mn doped ZnO using the standard solid state method and observed the antiferromagnetic nature of the doped samples [9]. Later, Sharma et al. first reported room temperature ferromagnetism in bulk Mn:ZnO synthesized by the solid state method at lower processing temperatures [10]. Mn doped polycrystalline ZnO system has been studied recently by many other research groups, and the observation of ferromagnetism at room temperature has been reported [11–14]. In recent reports, lattice defects have been shown to be responsible for high temperature ($T_C > 350$ K) ferromagnetism in (ZnMn)O nanoparticles [15–18]. However, it has also been shown that the secondary phase $Mn_{2-x}Zn_xO_{3-\delta}$, or an extrinsic source, is responsible for ferromagnetism in Mn doped ZnO [19,20], which was

* Corresponding author. Tel.: +91 20 2590 2273; fax: +91 20 2590 2636.
E-mail address: pa.joy@ncl.res.in (P.A. Joy).

0038-1098/$ - see front matter © 2007 Elsevier Ltd. All rights reserved.
doi:10.1016/j.ssc.2007.02.017

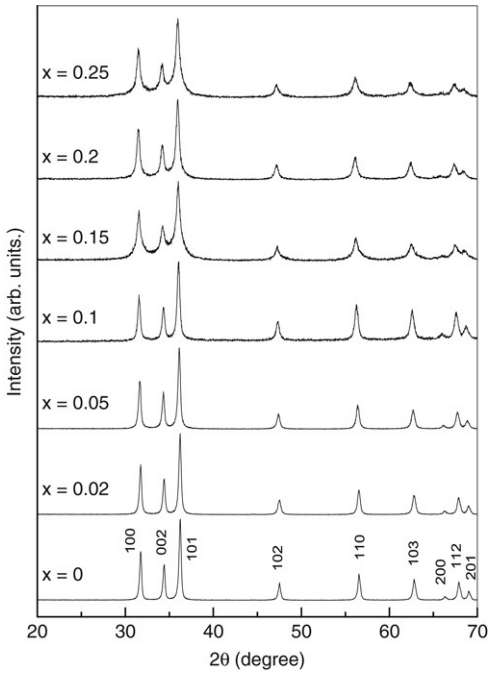

Fig. 1. Powder X-ray diffraction patterns of different compositions of $Zn_{1-x}Mn_xO$ ($0 \leq x \leq 0.25$).

initially thought to be intrinsic [10]. It has been shown that $Zn_{0.95}Mn_{0.05}O$, when synthesized by the solid state reaction at 1170 K, is ferromagnetic whereas annealing the sample at 1370 K destroys ferromagnetism [21]. The observed ferromagnetism is depicted to a secondary phase (Mn, Zn)Mn_2O_4. From the studies on polycrystalline $Zn_{1-x}Mn_xO$ system with different x values, it has been shown that the samples are either paramagnetic or antiferromagnetic [22–26]. Therefore, few research groups believe that secondary phases are responsible for ferromagnetism in doped ZnO, as the results are not always reproducible [27].

Liu et al. recently fabricated $Zn_{1-x}Mn_xO$ nanowires by a chemical vapor deposition method and found the Curie temperature to be as low as 44 K [28], close to the Curie temperature of Mn_3O_4. However, recently Philipose et al. reported room temperature ferromagnetism in (ZnMn)O nanowires grown on silicon substrates fabricated by a vapor–liquid–solid method [29]. Here, we report the synthesis of Mn doped ZnO in the form of nanowires using a simple and single step procedure involving an autocombustion method and their magnetic properties.

2. Experimental

Mn doped ZnO was synthesized by a combustion method from the nitrates of Zn and Mn taken in the appropriate ratio, using glycine as the fuel [30]. Zn and Mn metal powders were taken in stoichiometric amounts and dissolved separately in 4N HNO_3 and mixed together. To the above mixed metal nitrate solution, a water solution of 2 moles of glycine per mole of metal was added. The mixed solution was taken in a large crystallizing dish and kept over a hot plate for autocombustion at 473 K. After the complete evaporation

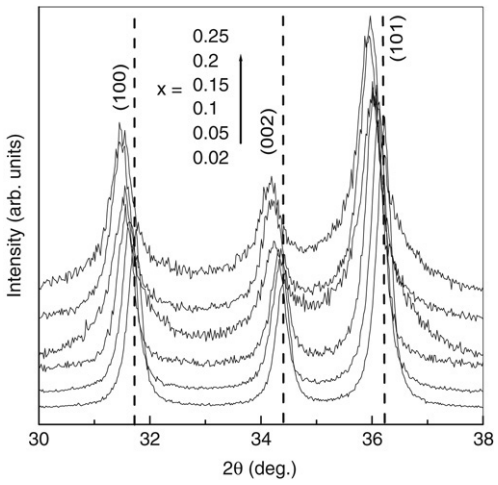

Fig. 2. Comparison of the expanded powder XRD patterns of different compositions in $Zn_{1-x}Mn_xO$ ($0 < x \leq 0.25$) in 30°–38° 2θ regions. The vertical dashed lines indicate the positions of the indexed reflections from ZnO.

of water, a reddish colored thick gel was formed, which was subsequently burnt to give a final brown colored oxide product. The as-synthesized powder samples thus obtained were characterized by powder X-ray diffraction (Philips 1730, Cu Kα radiation). The powder morphology was studied using a JEOL model 1200 EX transmission electron microscope. Magnetization measurements, as a function of magnetic field and temperature, were carried out using a vibration sample magnetometer (EG&G PAR 4500). Electronic absorption spectra were recorded on a JASCO V-570 spectrophotometer.

3. Results and discussion

The powder XRD patterns of different $Zn_{1-x}Mn_xO$ ($0 \leq x \leq 0.25$) samples are shown in Fig. 1. The XRD patterns for $x > 0$ show that the ZnO structure is not disturbed on substitution. No reflections due to any secondary phase are detected in the XRD patterns. The width of the reflections increase with increasing Mn content, indicating decreasing particle (crystallite) size. The average particle sizes were calculated from X-ray line broadening using the Scherrer formula [31]. A decrease in the average particle size with increasing Mn content is observed, and similar results are reported in the literature [23]. The average particle size obtained for different compositions of $Zn_{1-x}Mn_xO$ are 40, 27, 26, 21, 15, 18 and 15 nm for $x = 0$, 0.02, 0.05, 0.1, 0.15, 0.2 and 0.25, respectively. The expanded XRD patterns in the 30°–38° 2θ region, shown in Fig. 2, clearly indicate that the XRD reflections are shifted to lower 2θ values with increasing concentration of Mn. This is a proof of the incorporation of Mn ions inside the ZnO crystal lattice. The ionic radius of Zn^{2+} is 0.60 Å, and that of Mn^{2+} is 0.66 Å, for four-fold coordination [32]. Hence, Mn incorporation will lead to an expansion of the ZnO lattice. Fig. 3 shows the variation of the hexagonal lattice parameters with Mn concentration (x). The lattice parameter 'c' increases almost linearly with x, whereas 'a' increases up to 20% doping and becomes almost constant. A similar increase in the lattice parameters has been reported for (ZnMn)O by various researchers [21,33–35].

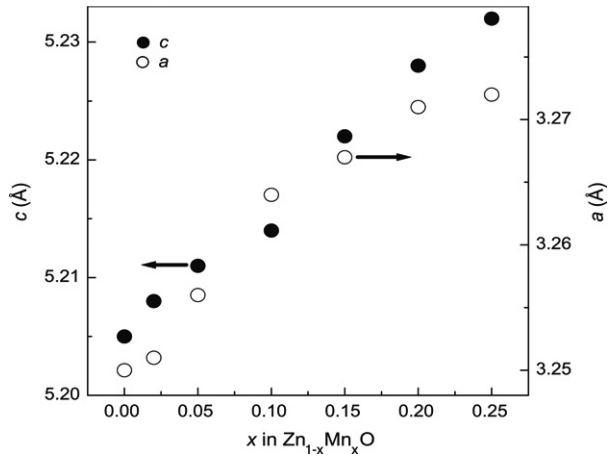

Fig. 3. Variation of the hexagonal lattice parameters (a and c) with Mn concentration for $Zn_{1-x}Mn_xO$ powder samples.

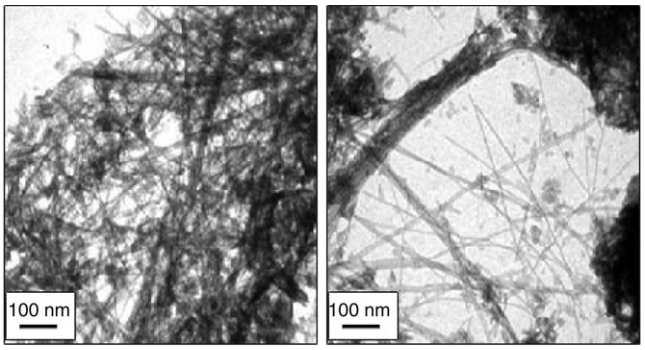

Fig. 4. TEM images of $Zn_{0.8}Mn_{0.2}O$ nanowires from two different regions.

The morphology of the as-synthesized sample of $Zn_{0.8}Mn_{0.2}O$ is shown in Fig. 4. Randomly aligned nanowires can be clearly seen in the micrographs. The diameter (d) of the nanowires is not uniform, but for all the nanowires, $d \leq 10$ nm. The lengths of the $Zn_{0.8}Mn_{0.2}O$ nanowires are found to be ~1 μm. The average particle size obtained from XRD (~18 nm) for $Zn_{0.8}Mn_{0.2}O$ nanowires is slightly larger when compared to the diameter (~10 nm) obtained from the TEM studies.

The room temperature optical absorption spectra of the various compositions in (ZnMn)O are shown in Fig. 5(a). Apart from the band gap transition, other optical absorption features are clearly seen for the doped samples at lower energies. A strong absorption band is seen at 2.94 eV (marked as 'p' in Fig. 5(a)). This is due to the spin forbidden ${}^6A_1(S) \rightarrow {}^4T_2(G)$ transition of Mn^{2+} in a tetrahedral environment. Such a type of strong spin forbidden transition is already reported for (ZnMn)O. This is explained in terms of the lattice distortion due to the incorporation of the larger Mn^{2+} ions inside the ZnO lattice [11,33,36,37]. Moreover, an increase in the absorption intensity is observed with increasing x. A very weak absorption is seen around 1.81 eV (marked as 'q' in Fig. 5(a)). This feature is not very clear for low doping concentrations, whereas it is slightly visible for the highly Mn doped samples. This absorption band is depicted as the spin-forbidden ${}^6A_1(S) \rightarrow {}^4T_1(G)$ (~15 200 cm^{-1}) transition [36].

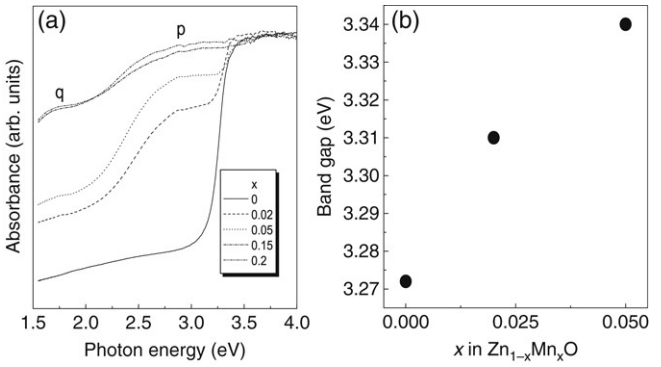

Fig. 5. (a) Optical absorption spectra for $Zn_{1-x}Mn_xO$ ($x = 0$, 0.02, 0.05, 0.15 and 0.2) powder samples, recorded at room temperature. (b) Variation of band gap of $Zn_{1-x}Mn_xO$ as a function of x.

Thus, optical absorption studies confirm the presence of Mn^{2+} ions in the tetrahedral sites. The band gaps for $x = 0$, 0.02 and 0.05 are shown in Fig. 5(b). The band gap values for the doped samples are obtained as 3.311 and 3.340 eV for $Zn_{0.98}Mn_{0.02}O$ and $Zn_{0.95}Mn_{0.05}O$, respectively. Similar enhancement of the band gap with increasing Mn concentration has been reported earlier [33–35,37]. The blue shift of the band edge, presence of Mn^{2+} ions in the tetrahedral sites, and the increased hexagonal lattice parameters are some indicators of the incorporation of Mn ions inside the ZnO lattice.

The magnetization of the different samples is measured as a function of field at room temperature and 12 K as well as a function of temperature at a fixed field strength. All the Mn doped samples were found to be paramagnetic at room temperature. The temperature variations of the magnetization of $Zn_{0.9}Mn_{0.1}O$, $Zn_{0.8}Mn_{0.2}O$ and $Zn_{0.75}Mn_{0.25}O$ are shown in Fig. 6. The applied magnetic field in each case was 5000 Oe. All the three samples show similar features. A rapid increase in the magnetization is observed below ~50 K for all the three samples. The inverse of the magnetic susceptibility of two different samples are shown in the inset of Fig. 6. From the nature of the inverse susceptibility curves, it is likely that the samples are either ferromagnetic or ferrimagnetic at low temperatures. A typical Curie–Weiss behavior is observed above 100 K for the samples. A least squares fit of the linear portion of the curves above 100 K gave a negative Weiss temperature (Θ) for both samples. The value of Θ is obtained as −164 K and −212 K for $Zn_{0.8}Mn_{0.2}O$ and $Zn_{0.75}Mn_{0.25}O$, respectively. The high negative values of Θ indicate either strong antiferromagnetic or ferrimagnetic interactions in these Mn doped samples. An antiferromagnetic nature for the samples can be ruled out from the shape of the susceptibility curves. The effective paramagnetic moment (μ_{eff}) per Mn, is derived for these two samples, using the equation, $\mu_{\text{eff}} = 2.828\sqrt{C}$, where C is the Curie constant obtained from the slope of $1/\chi$ vs. T curve above 100 K. For both the samples, μ_{eff} is obtained as ~5.8μ_B, which is close to 5.9μ_B for Mn^{2+} [24,35]. The μ_{eff} value indicates that the oxidation state of Mn is 2+. The results from the magnetic measurements are in agreement with those reported in the literature for $Zn_{1-x}Mn_xO$ samples. Very large negative values of Θ, along with a deviation from linearity below ~50 K similar

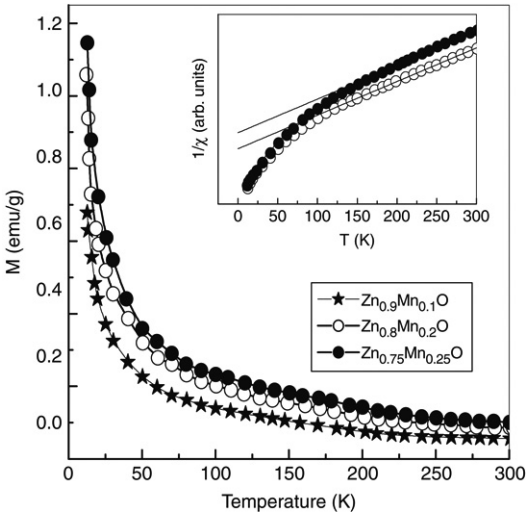

Fig. 6. Temperature variation of magnetization of $Zn_{1-x}Mn_xO$ ($x = 0.1$, 0.2 and 0.25) powder samples. Inset: Reciprocal susceptibility vs. temperature of $Zn_{0.8}Mn_{0.2}O$ and $Zn_{0.75}Mn_{0.25}O$.

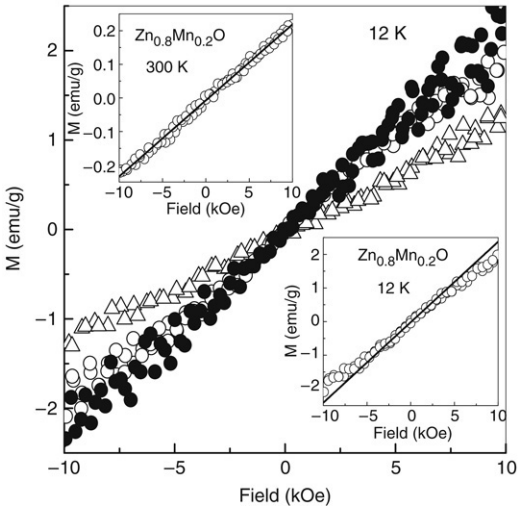

Fig. 7. Magnetization of the Mn substituted compositions as a function of field, measured at 12 K. △ $x = 0.05$, ○ $x = 0.2$, ● $x = 0.25$. Insets: M–H curve of $Zn_{0.8}Mn_{0.2}O$ at 12 K and 300 K. The solid lines are intended to show the linearity of the data.

to that observed in the present work, are reported [6,23,26,38], suggesting strong antiferromagnetic couplings. However, considering the large increase in the magnetization below 50 K and the large negative value of the Weiss temperature, it can be considered that the samples are ferrimagnetic.

Fig. 7 shows M–H curves of $Zn_{1-x}Mn_xO$ ($x = 0.05$, 0.2 and 0.25) measured at 12 K. The magnetization curves are almost linear with field strength. However, a closer examination of the magnetization curves, as shown in the insets of Fig. 7 for $Zn_{0.8}Mn_{0.2}O$, reveals that the sample is paramagnetic at room temperature (M vs. H is linear), whereas it is not truly paramagnetic at 12 K. A large deviation from the expected paramagnetic behavior is observed for higher fields in the 12 K data. This is possible if the sample is superparamagnetic or is a mixture of a major paramagnetic and a minor ferro/ferrimagnetic phases. The absence of a hysteresis loop indicates superparamagnetic behavior.

There are several reports in the literature where Mn-doped ZnO samples are found to be magnetic below 50 K with T_C close to 40 K. The large low temperature magnetization in the (ZnMn)O system has been attributed to various effects, such as carrier mediated ferromagnetism [28,39], the presence of a ferromagnetic Mn_3O_4 phase [40,41], the presence of a secondary Zn substituted spinel $(MnZn)Mn_2O_4$ phase [14,21], spin freezing [42], etc. From the studies on Mn doped ZnO on different substrates, Mofor et al. [43] have shown that there can also be contributions from the substrate on the observed ferromagnetism. In the present case, since the XRD studies did not show any evidence for the presence of secondary phases, the origin of ferro/ferrimagnetism can be intrinsic or because of defects. However, the presence of secondary phases in very small quantities cannot be ruled out if the amount present is less than the detection limit of XRD. Moreover, the maximum intense peak of the possible spinel-type impurity phase Mn_3O_4 (311) overlaps with the maximum intense peak of ZnO (101), and hence cannot be differentiated from it if present in small amounts.

Magnetic characteristics like ferromagnetism at room temperature, ferromagnetism at low temperatures in the samples which are paramagnetic at room temperature, and the absence of ferromagnetism at all temperatures have been reported previously for polycrystalline samples of Mn doped ZnO. Interestingly, the polycrystalline samples are synthesized by different methods in the different reports, and the results are reproducible whenever the same method is followed. In the present work, the polycrystalline samples are synthesized by a combustion method. This method has been shown to be suitable for the synthesis of single phase multicomponent oxides [44]. Earlier, we have shown that it is possible to synthesize and stabilize metastable phases of some perovskite oxides by this method, when it is not possible to stabilize these phases by other methods [45,46]. However, the combustion method is highly susceptible to producing different results, depending on the nature of the fuel used in the reaction as well as the ratio of the fuel to the oxidizer. In the case of Co doped ZnO, it has been shown that both ferromagnetism and paramagnetism at room temperature can be obtained by slightly modifying the synthesis conditions where ferromagnetism was found to be due to the presence of impurity phases [47]. In the present work, it is possible that the observed magnetic characteristics at low temperatures are likely to be either due to the intrinsic behavior from some defect structures created because of the particular synthesis conditions, or due to the presence of minor impurity phases. Further detailed work is required to understand this.

4. Conclusions

Single phase $Zn_{1-x}Mn_xO$ ($0 \leq x \leq 0.25$) nanowires have been synthesized using a simple combustion method. With the increasing content of Mn, lattice parameters of doped ZnO increase due to the larger ionic radius of Mn^{2+}. Optical absorption investigations reveal the presence of Mn^{2+}

in tetrahedral coordination, possibly due to the substitution of Mn for Zn in the ZnO lattice. All samples are paramagnetic at room temperature, and the susceptibility data give evidence for strong antiferromagnetic interactions. A large increase in the magnetization below 50 K and nonlinear M–H behavior at 12 K indicate that the samples are ferrimagnetic at low temperatures. However, the presence of small fractions of other ferrimagnetic impurities in the paramagnetic samples cannot be ruled out.

Acknowledgement

S. Deka is grateful to the University Grants Commission, Govt. of India, for a Research Fellowship.

References

[1] K. Sato, H. Katayama-Yoshida, Japan. J. Appl. Phys. Part 2 39 (2000) L555.
[2] T. Dietl, H. Ohno, F. Matsukura, J. Cibert, D. Ferrand, Science 287 (2000) 1019.
[3] S.J. Pearton, C.R. Abernathy, M.E. Overberg, G.T. Thaler, D.P. Norton, N. Theodoropoulou, A.F. Hebard, Y.D. Park, F. Ren, J. Kim, L.A. Boatner, J. Appl. Phys. 93 (2003) 1.
[4] R. Janisch, P. Gopal, N.A. Spaldin, J. Phys.: Condens. Matter 17 (2005) R657.
[5] Z. Jin, T. Fukumura, M. Kawasaki, K. Ando, H. Saito, T. Sekiguchi, Y.Z. Yoo, M. Murakami, Y. Matsumoto, T. Hasegawa, H. Koinuma, Appl. Phys. Lett. 78 (2001) 3824.
[6] T. Fukumura, Z. Jin, M. Kawasaki, T. Shono, T. Hasegawa, S. Koshihara, H. Koinuma, Appl. Phys. Lett. 78 (2001) 958.
[7] J.M.D. Coey, M. Venkatesan, C.B. Fitzgerland, Nature Mater. 4 (2005) 173.
[8] N.H. Hong, J. Sakai, V. Brize, J. Phys.: Condens. Matter 19 (2007) 036219.
[9] S. Kolesnik, B. Dabrowski, J. Mais, J. Supercond. 15 (2002) 251.
[10] P. Sharma, A. Gupta, K.V. Rao, F.J. Owens, R. Sharma, R. Ahuja, J.M.O. Guillen, B. Johansson, G.A. Gehring, Nature Mater. 2 (2003) 673.
[11] N.S. Norberg, K.R. Kittilstved, J.E. Amonette, R.K. Kukkadapu, D.A. Schwartz, D.R. Gamelin, J. Am. Chem. Soc. 126 (2004) 9387.
[12] K.R. Kittilstved, N.S. Norberg, D.R. Gamelin, Phys. Rev. Lett. 94 (2005) 147209.
[13] D.P. Joseph, G.S. Kumar, C. Venkateswaran, Mater. Lett. 59 (2005) 2720.
[14] O.D. Jayakumar, H.G. Salunke, R.M. Kadam, M. Mohapatra, G. Yaswant, S.K. Kulshreshtha, Nanotechnology 17 (2006) 1278.
[15] K.R. Kittilstved, D.R. Gamelin, J. Am. Chem. Soc. 127 (2005) 5292.
[16] K.R. Kittilstved, W.K. Liu, D.R. Gamelin, Nature Mater. 5 (2006) 291.
[17] J.B. Wang, G.J. Huang, X.L. Zhong, L.Z. Sun, Y.C. Zhou, E.H. Liu, Appl. Phys. Lett. 88 (2006) 252502.
[18] D. Rubi, A. Calleja, J. Arbiol, X.G. Capdevila, M. Segarra, Ll. Aragones, J. Fontcuberta, http://xxx.lanl.gov/pdf/cond-mat/0608014.
[19] D.C. Kundaliya, S.B. Ogale, S.E. Lofland, S. Dhar, C.J. Metting, S.R. Shinde, Z. Ma, B. Varughese, K.V. Ramanujachary, L. Salamanca-Riba, T. Venkatesan, Nature Mater. 3 (2004) 709.
[20] K.P. Bhatti, S. Chaudhary, D.K. Pandya, S.C. Kashyap, Solid State Commun. 140 (2006) 23.
[21] S.-J. Han, T.-H. Jang, Y.B. Kim, B.-G. Park, J.-H. Park, Y.H. Jeong, Appl. Phys. Lett. 83 (2003) 920.
[22] S. Kolesnik, B. Dabrowski, J. Mais, J. Appl. Phys. 95 (2004) 2582.
[23] J. Luo, J.K. Liang, Q.L. Liu, F.S. Liu, Y. Zhang, B.J. Sun, G.H. Rao, J. Appl. Phys. 97 (2005) 086106.
[24] G. Lawes, A.S. Risbud, A.P. Ramirez, R. Seshadri, Phys. Rev. B 71 (2005) 045201.
[25] C.N.R. Rao, F.L. Deepak, J. Mater. Chem. 15 (2005) 573.
[26] W. Chen, L.F. Zhao, Y.Q. Wang, J.H. Miao, S. Liu, Z.C. Xia, S.L. Yuan, Solid State Commun. 134 (2005) 827.
[27] R. Seshadri, Curr. Opin. Solid State Mater. Sci. 9 (2005) 1.
[28] J.J. Liu, M.H. Yu, W.L. Zhou, Appl. Phys. Lett. 87 (2005) 172505.
[29] U. Philipose, S.V. Nair, S. Trudel, C.F. de Souza, S. Aouba, R.H. Hill, H.E. Ruda, Appl. Phys. Lett. 88 (2006) 263101.
[30] S. Deka, P.A. Joy, Chem. Mater. 17 (2005) 6507.
[31] B.D. Cullity, Elements of X-Ray Diffraction, 2nd ed., Addison-Wesley, Massachusetts, 1978.
[32] R.D. Shannon, Acta Cryst. A 32 (1976) 751.
[33] T. Fukumura, Z. Jin, A. Ohtomo, H. Koinuma, M. Kawasaki, Appl. Phys. Lett. 75 (1999) 3366.
[34] S.W. Jung, S.-J. An, G.-C. Yi, C.U. Jung, S.-I. Lee, S. Cho, Appl. Phys. Lett. 80 (2002) 4561.
[35] A. Tiwari, C. Jin, A. Kvit, D. Kumar, J.F. Muth, J. Narayan, Solid State Commun. 121 (2002) 371.
[36] C.H. Bates, W.B. White, R. Roy, J. Inorg. Nucl. Chem. 28 (1966) 397.
[37] Z. Jin, M. Murakami, T. Fukumura, Y. Matsumoto, A. Ohtomo, M. Kawasaki, H. Koinuma, J. Cryst. Growth 214–215 (2000) 55.
[38] H.-W. Zhang, E.-W. Shi, Z.Z. Chen, X.-C. Liu, B. Xiao, Solid State Commun. 137 (2006) 272.
[39] Y.Q. Chang, D.B. Wang, X.H. Luo, X.Y. Xu, X.H. Chen, L. Li, C.P. Chen, R.M. Wang, J. Xu, D.P. Yu, Appl. Phys. Lett. 83 (2003) 4020.
[40] Y.M. Kim, M. Yoon, I.-W. Park, Y.J. Park, Jong H. Lyou, Solid State Commun. 129 (2004) 175.
[41] J. Zhang, R. Skomski, D.J. Sellmyer, J. Appl. Phys. 97 (2005) 10D303.
[42] A.B. Mahmoud, H.J. von Bardeleben, J.L. Cantin, E. Chikoidze, A. Mauger, J. Appl. Phys. 101 (2007) 013902.
[43] A.C. Mofor, A. El-Shaer, A. Bakin, A. Waag, H. Ahlers, U. Siegner, S. Sievers, M. Albrecht, W. Schoch, N. Izyumskaya, V. Avrutin, S. Sorokin, S. Ivanov, J. Stoimenos, Appl. Phys. Lett. 87 (2005) 062501.
[44] L.A. Chick, L.R. Pederson, G.D. Maupin, J.L. Bates, L.E. Thomas, G.J. Exarhos, Mater. Lett. 10 (1990) 6.
[45] P.A. Joy, Y.B. Khollam, S.K. Date, Phys. Rev. B 62 (2000) 8608.
[46] V.L.J. Joly, P.A. Joy, S.K. Date, Phys. Rev. B 65 (2002) 184416.
[47] S. Deka, R. Pasricha, P.A. Joy, Phys. Rev. B 74 (2006) 033201.